



## Full length article

## Distance to the water table shapes the diversity and activity of DNA and RNA viruses in a subalpine peatland



Ziye Xiong<sup>a</sup>, Xuan Qiu<sup>a,\*</sup>, Xing Xiang<sup>b</sup>, Lanlan Cai<sup>c</sup>, Nian Wang<sup>d</sup>, Xianyu Huang<sup>a</sup>, Hongmei Wang<sup>a</sup>

<sup>a</sup> State Key Laboratory of Geomicrobiology and Environmental Changes, China University of Geosciences (Wuhan), Wuhan 430078, China

<sup>b</sup> College of Life Science, Shangrao Normal University, Shangrao 334099, China

<sup>c</sup> Earth, Ocean and Atmospheric Sciences Thrust, The Hong Kong University of Science and Technology (Guangzhou), Guangzhou 511453, China

<sup>d</sup> BGI Research, Wuhan 430074, China

## ARTICLE INFO

Handling Editor: Adrian Covaci

## Keywords:

Viromics  
Metatranscriptomics  
 $\text{CH}_4$  cycle  
Auxiliary metabolic genes  
Water table

## ABSTRACT

Peatlands are essential reservoirs of carbon and critical zones for the cycling of greenhouse gases on Earth. Their ecological functions are primarily governed by the microbial communities inhabiting them, which vary with hydrological conditions. However, the roles of viruses in peatland ecosystems remain poorly understood despite their abundance and ubiquity. To address this gap, viral communities, their ecological roles, and their responses to environmental factors were explored using viromics, metatranscriptomics, and physicochemical property analyses of nine peat sediments collected from various layers of three profiles with different water table levels in the Dajiuju Peatland, central China. This study revealed that the distance to the water table (DWT) significantly influenced the composition and function of viral communities by altering the levels of redox potential and total organic carbon, which in turn affected methane ( $\text{CH}_4$ ) concentrations in pore water. Furthermore, a notable abundance of putative auxiliary metabolic genes associated with methane, nitrogen, and sulfur metabolism was identified in peatland DNA viruses, with their community composition strongly regulated by DWT. Additionally, functional genes related to oxidative phosphorylation and cysteine synthesis were detected for the first time in peatland RNA viruses. This study advances our comprehension of how hydrological conditions affect viral communities in peatlands, provides new insights into the impact of viruses on the  $\text{CH}_4$  cycle, and serves as a crucial reference for future investigations into the ecological roles of viruses.

## 1. Introduction

Peatlands are essential to the global carbon cycle, storing approximately 30 % of the world's soil carbon while covering only 3 ~ 4 % of the Earth's land surface (Leifeld and Menichetti, 2018). This remarkable carbon storage capacity highlights their vital role in regulating the levels of atmospheric greenhouse gases, such as  $\text{CH}_4$  and  $\text{CO}_2$ , thereby playing a significant role under the climate change scenario (Evans et al., 2021; Yu et al., 2011).

Microbial communities within peatlands are crucial drivers of biogeochemical processes, including the cycling of carbon, nitrogen, sulfur, phosphorus, etc., with  $\text{CH}_4$  cycling receiving the most attention. Methanogenic archaea produce  $\text{CH}_4$ , while methanotrophic bacteria oxidize most of the  $\text{CH}_4$  to  $\text{CO}_2$  before it escapes into the atmosphere (Lyu et al., 2018; Thauer, 2010). The net  $\text{CH}_4$  flux from peatlands is

regulated by the activity and diversity of methanogens and methanotrophs, which are primarily influenced by redox conditions and substrate availability within peat sediments (Wang et al., 2022b). Previous studies have demonstrated that the microbial community in peatlands fluctuates across the vertical peat profiles characterized by steep physicochemical gradients, resulting in variation in microbially mediated biogeochemical cycling. Among these physicochemical parameters, the water table level has emerged as the predominant factor influencing  $\text{CH}_4$  cycling (Evans et al., 2021). High water tables create anoxic conditions conducive to methanogenesis, whereas lower water tables promote aerobic conditions that generally enhance methanotrophic activity (Liu et al., 2022). Notably, existing studies have demonstrated that the mean annual effective water table depth influences  $\text{CH}_4$  and  $\text{CO}_2$  emissions more than any other management-related factors in peat environments, emphasizing the importance of hydrological management in controlling

\* Corresponding author.

E-mail address: [qiu.xuan@cug.edu.cn](mailto:qiu.xuan@cug.edu.cn) (X. Qiu).

greenhouse gas fluxes (Evans et al., 2021; Huang et al., 2021). The water table dynamics may govern the unique diversity and co-occurrence patterns of key microbial functional groups involved in CH<sub>4</sub> cycling (Tian et al., 2024).

In addition to the above typical cellular microbes, non-cellular microbes—viruses, are also essential biological entities due to their vast abundance and significant role in regulating microbial communities through lysis of host cells, modulation of microbial activity, and horizontal gene transfer (Trubl et al., 2018). For instance, viruses are involved in cell growth regulation and stress responses through expressing the related auxiliary metabolic genes (AMGs) (Luo et al., 2022). Moreover, increasing evidence illustrates that viruses may play roles in various biogeochemical cycles. Some DNA viruses with large genomes have been reported to carry the *pmoC* gene (Chen et al., 2020), exhibiting significant potential to influence the CH<sub>4</sub> oxidation and carbon cycle. Although previous studies have shown that the structural and functional characteristics of viral community varied with habitats and environmental factors in wetlands, soils, oceans, etc., (Gregory et al., 2019; Zhu et al., 2024; Zhu et al., 2023), the understanding of how viruses respond to variations in hydrological conditions and the subsequent effects on CH<sub>4</sub> cycling in peatland ecosystems remains limited.

In contrast to the research surge in the ecological roles of DNA viruses, studies on RNA viruses were mainly conducted in the context of animal and plant diseases (Liang et al., 2023; Woolhouse and Brierley, 2018). However, some works suggest that RNA viruses may be as abundant as, or even exceed, DNA viruses in marine ecosystems (Steward et al., 2013; Urayama et al., 2018), and the catalogs of RNA viruses have recently been significantly expanded through the analysis of global RNA-directed RNA polymerase (RdRp) sequences (Zayed et al., 2022). The high abundance and diversity of marine RNA viruses may indicate their critical ecological significance in the environments. Some studies found that RNA viruses could affect host photosynthesis and carbon cycling processes, potentially leading to profound impacts on marine carbon emissions (Dominguez-Huerta et al., 2022). Additionally, current evidence suggests that the primary evolutionary pathway of RNA viruses involves drastic host shifts, even crossing the divide between prokaryotes and eukaryotes, which further suggests that the impacts of RNA viruses on ecosystems may be complex and diverse (Neri et al., 2022). Compared to marine ecosystems, there remains a lack of comprehensive understanding of RNA viruses in wetland ecosystems, particularly in peat environments. Furthermore, existing wetland research has primarily focused on the diversity and potential ecological functions of viruses and key microorganisms, with few focus on the association between microbial activity and viral activity, which significantly constrains the understanding of the ecological role of viruses.

In this study, we employed metatranscriptomics and viromics to investigate the community composition of DNA and RNA viruses in the Dajiuju peatland across various distances from the water table (DTW), as well as their environmental drivers. We also explored the potential ecological functions of viruses in the Dajiuju peatland, especially related to the CH<sub>4</sub> cycle. In light of global warming, this study provides new insights into the roles of viruses in carbon storage and emission in peatlands with varying water table levels particularly enhancing our understanding of microbially modulated CH<sub>4</sub> cycling in peatland ecosystems.

## 2. Materials and methods

### 2.1. Study site

The Dajiuju peatland (109°59'46.99"E, 31°29'26.7"N), a typical subalpine peatland, is located in the Shennongjia Forestry District, Hubei Province, central China. With an average elevation of 1,730 m (Li et al., 2016b) and under the influence of the subtropical monsoon climate, this area experiences intense rainfall from April to September, with an annual average precipitation of 1,560 mm (Huang et al., 2013).

The water table depth (WTD) in the Dajiuju peatland varies significantly due to the basin's undulating topography. The plant community in the peatland is diverse, characterized by *Sphagnum palustre* and various companion species (Tian et al., 2019).

### 2.2. Sampling and physicochemical characterization

Three sites with varying WTD were selected for sampling and designated as L (low), M (medium), and H (high) in April 2023. Exact WTD values were measured from sediment profiles excavated at each sampling site (Fig. S1). A positive WTD value indicates that the water table is below the peat surface, while a negative WTD value indicates that it is above the peat surface. On each profile, sediment samples were taken from layers at depths of -32 to -27 cm, -5 to 0 cm, 15 to 20 cm, and 45 to 50 cm relative to the water table. The negative values indicate layers above the water table, while the positive values represent layers below the water table. Notably, two (H1 and H2), three (M1, M2, and M3), and four layers (L1, L2, L3, and L4) were present at high, medium, and low WTD sites, respectively (Fig. S1). Approximately 500 g of sediments were collected from each layer, with three replicates per layer. These samples were then transferred into sterilized plastic bags, mixed evenly in their bags, and preserved in a container with dry ice. Additionally, the pore water in corresponding layers was collected using soil solution samplers (MacroRhizon, NLD, Rhizosphere Research Products Company) and immediately stored in anoxic, sealed containers.

The physicochemical properties of peat sediments and pore water were analyzed. The dissolved organic carbon (DOC) concentration of peat sediments was quantified by a TOC analyzer (Elementar Vario, Germany). The water content (WC) was calculated by the sample weights before and after freeze-drying. The total organic carbon (TOC) and inorganic carbon (IC) were quantified by combustion method (TOC-L CPH, Shimadzu, Japan). For pore water, field measurements were taken for pH, redox potential (Eh) and conductivity using a multi-parameter water quality detector (HACH, Loveland, USA), while laboratory analyses were conducted for the concentrations of methane dissolved in the pore water (Water-CH<sub>4</sub>), Fe<sup>2+</sup>, and hydroxyl radical (-OH). More details were described in the Supplementary Material, and the physical and chemical parameters are shown in Table S1.

### 2.3. Metagenomic analysis for DNA viruses

#### 2.3.1. Viral particle enrichment, DNA extraction and sequencing

Virus-like particles were extracted from 9 peat samples following the methods described by Trubl et al. (Trubl et al., 2019) and ter Horst et al. (ter Horst et al., 2021), with several modifications. Briefly, 60 g of peat from each sample was evenly divided into six 50 mL Corning tubes. The peat in each tube was suspended in 15 mL of Amended Potassium Citrate Prime buffer (AKC'), which consists of 1 % K-citrate, 150 mM MgSO<sub>4</sub>, and 10 % PBS, resulting in a total of 90 mL of leaching solution per sample. The tubes were manually shaken for 30 s, followed by vortexing at 400 RPM for 20 min. The suspension was then centrifuged at 6,484 RPM (4,700 × g) for 20 min at 4 °C and subsequently filtered through 0.45 µm and 0.22 µm sterile polyethersulfone filters (Millex-GP). The viruses in the filtrate were concentrated using an ultra-speed centrifuge (Beckman SW-41 Ti) at 32,000 RPM (198,200 × g) for 3 h at 4 °C. The pellets from six tubes derived from the same sample were resuspended and combined with 500 µL of CD1 solution (QIAGEN, Germany), and transferred into a tube containing beads from the QIAGEN DNeasy PowerSoil Kit. Viral DNA was subsequently extracted according to the manufacturer's instructions (QIAGEN DNeasy PowerSoil Kit, Germany), with the exception that the vortexing step was replaced by incubation at 70 °C for 5 min in the second step.

DNA libraries were constructed according to the manufacturer's instructions (Illumina, USA). Briefly, index-coded samples were clustered using a cBot Cluster Generation System, and the resulting libraries were sequenced on a NovaSeq 6000 platform with a 150 bp paired-end

sequencing strategy provided by Berry Genomics Company (Beijing, China). Each sample was sequenced to a depth of 15 Gb.

### 2.3.2. Reads processing, DNA viral contigs identification, clustering, and abundance calculation

For the DNA virome analysis, paired raw reads were first quality-trimmed to remove low-quality reads and adapters using fastp v0.23.4 (Chen et al., 2018) (parameters:  $-5 -W 50 -M 20 -l 100 -n 0$ ). High-quality reads from each sample were then individually assembled using MEGAHIT v1.2.9 (Li et al., 2016a) with default parameters, except for ' $-min-contig-len 1500$ '.

Contigs longer than 5,000 bp were analyzed with DeepVirFinder (Ren et al., 2020) (scores  $> 0.9$  and  $p < 0.05$ ) and VirSorter2 (Guo et al., 2021) ( $-include-groups dsDNAPhage, ssDNA -min-score 0.5$ ) to identify putative viral sequences based on machine learning and viral hallmark gene identification methods. The quality and completeness of viral sequences were assessed using CheckV v1.0.1 (Nayfach et al., 2020). Only contigs containing at least one viral gene and not identified as prophages by CheckV v1.0.1 were retained (Zhu et al., 2023).

The confirmed DNA viral contigs from each sample were clustered into viral operational taxonomic units (vOTUs) using MMseqs2 v15.6 (Steinegger and Söding, 2017) with 95 % nucleotide identity and 85 % coverage in the "easy-linclust" mode (parameters:  $-min-seq-id 0.95, -cov-mode 1, -c 0.85$ ). To calculate the relative abundance of DNA viruses, clean reads from the DNA virome were mapped to viral contigs using BWA v0.7.17 with BWA-MEM algorithm (Li and Durbin, 2009), and then normalized to TPM (Transcripts Per Kilobase of Exon model per Million mapped reads) values. The coverage of per viral contig was calculated using BBMap (<https://sourceforge.net/projects/bbmap/>).

### 2.3.3. Taxonomic assignment, host prediction and comparison of virus sequences

Given the recent update to the ICTV classification system, DNA vOTUs were taxonomically classified using GeNomad v1.7.4 (Camargo et al., 2023) and PhaGCN2 (Jiang et al., 2022), and the annotation results from PhaGCN2 were performed manually to remove the non-DNA viruses. Virus-host links were predicted using iPhoP v1.3.3 (Roux et al., 2022) with a minimum confidence score cut-off of 90. In detail, all the links were established based on multiple criteria: (i) sequence comparison to host genomes and CRISPR spaces, (ii) overall nucleotide composition to host genomes, and (iii) comparison to viral genomes with known hosts. Given that virus-host infection relationships are often not singular, all results exceeding the predefined score threshold were retained. Viral sequences from this study, Stordalen Mire peatland (Emerson et al., 2018) and SPRUCE peatland (ter Horst et al., 2021) were collected to build a gene-sharing network using vConTACT2 v0.11.3 (Jang et al., 2019) with default parameters.

### 2.3.4. AMG identification, annotation and abundance calculation

Open reading frames (ORFs) of vOTU sequences were predicted using Prodigal v2.6.3 (Hyatt et al., 2010) with the parameters " $-p meta -f gff -q -m$ ". To avoid false AMG identification due to host contamination, two methods were employed to identify viral proteins: (1) CheckV v1.0.1 with its viral-specific HMM profiles and default parameters, followed by manual selection of viral genes, and (2) HMMsearch against the Prokaryotic Virus Orthologous Groups (pVOGs, release 5) (E-value  $\leq 1e^{-5}$  and bit score  $\geq 50$ ) (Graziotin et al., 2017; Luo et al., 2022). Only functional genes located between or adjacent to viral genes were considered candidate AMGs (Pratama et al., 2021). Putative AMGs were annotated using the KEGG database with eggNOG-mapper v2.1.12 (Cantalapiedra et al., 2021). Since many viral AMGs are derived from the host, the relative abundance of AMGs was represented by the abundance of vOTUs carrying these AMGs in each sample to alleviate interference from host sequences.

## 2.4. Metagenomic analysis for RNA viruses

### 2.4.1. Total RNA extraction, quality control and downstream analysis

Total RNA was extracted from 2 g of peat using the RNA PowerSoil® Total RNA Isolation Kit (12866–25, MoBio, USA) according to the manufacturer's instructions. RNA integrity was assessed using an Agilent Bioanalyzer 2100 (Agilent, USA). The ribosomal RNA was subsequently removed using Ribo-Zero rRNA Removal Kit (Illumina). Reverse transcription and metatranscriptomic sequencing library construction were performed using Illumina's TruSeq Stranded mRNA LT Sample Prep Kit (Illumina, USA). Each library was sequenced on an Illumina NovaSeq platform (Illumina, USA) using the PE150 strategy at Personal Biotechnology Co., Ltd. (Shanghai, China), achieving a sequencing depth of 15 Gb per sample.

For the metatranscriptomic analysis, raw sequencing reads were initially processed with Cutadapt v1.17 (Martin, 2011) to remove sequencing adapters. Low-quality reads were then trimmed using fastp v0.23.4 (Chen et al., 2018) with a sliding-window algorithm. Ribosomal RNA was removed using SortMeRNA (v4.2.0) (Kopylova et al., 2012) with the default rRNA reference database. All quality-filtered reads were assembled using MEGAHIT v1.2.9 (Li et al., 2016a). Protein-coding genes in assembled contigs longer than 300 bp were predicted using Prodigal v2.6.3 (Hyatt et al., 2010), following the methods described in Section 2.3.4. These proteins were then compared using Diamond BLASTp (Buchfink et al., 2015) against the NR database (downloaded on February 7, 2024) to reveal the microbial community composition.

RNA viruses were identified from the assembled contigs using two approaches. First, based on hidden Markov models (HMMs) generated from alignments published by Neri et al. (Neri et al., 2022), all protein-coding genes were screened for viral RdRp domain protein sequences using HMMSearch v3.4 (Finn et al., 2011). Contigs were retained only if they encoded RdRp proteins with E-values  $\leq 1e^{-10}$  and scores  $> 50$ . Second, assembled contigs without RdRp hits from each library were verified through protein searches against the NCBI NR database using Diamond BLASTp (Buchfink et al., 2015) with E-value  $\leq 1e^{-5}$ . Contigs were excluded if any protein exhibited a top hit matching cellular organisms or DNA viruses. The relative abundance of identified RNA viral contigs was calculated using the method described in Section 2.3.2.

Taxonomic classification of the identified RNA viral contigs was performed using two approaches. For contigs containing the RdRp gene, classification was on HMMsearch alignment results. Contigs with hits from multiple RdRp-based viral groups were assigned to the taxon with the lowest E-value. At the family level, classification was further refined based on amino acid sequence similarity, with thresholds set at 50 % identity and 50 % query coverage (Liu et al., 2024). For incomplete contigs lacking RdRp genes, taxonomic classification relied on their protein matches with the NCBI NR database, retaining results with the lowest E-value.

The functional annotation of proteins within RNA viral contigs was conducted using the method outlined in Section 2.3.4.

### 2.4.2. Phylogenetic analysis

RdRp sequences from three previously published studies (Hillary et al., 2022; Starr et al., 2019; Wolf et al., 2018) were processed using the same methods described in Section 2.4.1. To construct a phylogenetic tree of RdRp proteins, sequences were clustered using MMseqs2 at 100 % nucleotide identity. Representative RdRp sequences were aligned using MAFFT v7.525 (Katoh et al., 2002), and all alignments were trimmed using TrimAl v1.4.1 (parameters:  $-gappyout$ ) (Capella-Gutierrez et al., 2009). The maximum likelihood tree was then constructed using IQ-Tree v2.3.3 (Minh et al., 2020) and visualized using Chiplot (Xie et al., 2023).

## 2.5. Statistical analysis

Statistical analysis and visualization were performed using R v4.3.3

(<https://www.R-project.org/>) and Chipplot (<https://www.chiplot.online/>). The relative abundance in this study was calculated based on transcript abundance (TPM), and the normalized abundance matrix was generated as input for subsequent analyses.  $\alpha$ -diversity metrics of viral communities were calculated using the R package vegan. Non-metric multidimensional scaling (NMDS) analysis was used to assess the distance between viral communities based on the Bray-Curtis distance. The statistical significance of differences between groups was assessed using Permutational Multivariate Analysis of Variance (PERMANOVA). The relationships between environmental factors and viral communities, as well as AMGs, were revealed by the Mantel tests. Partial Least Squares Path Modeling (PLS-PM) was used to assess the direct and indirect effects of environmental factors on the  $\alpha$  and  $\beta$  diversity of viral communities. The Shannon index was used to measure  $\alpha$ -diversity, while the first axis of NMDS analysis based on the Bray-Curtis dissimilarity matrix represented  $\beta$ -diversity. Path coefficients and  $R^2$  values in the path model were computed using the plspm package.

### 3. Results

#### 3.1. Overview of DNA/RNA viral communities and diversity across different DWTs

From the DNA virome, a total of 41,451 DNA viral contigs  $\geq 5$  kb were identified and clustered into 15,073 species-level viral populations (vOTUs) based on 95 % nucleotide identity and 85 % coverage. Among these vOTUs, 374 (2.5 %) of them were classified as high-quality ( $>90$  % complete) or complete using CheckV (Table S2). The taxonomically classified vOTUs were assigned into 8 classes, 25 orders, and 96 families according to the latest ICTV classification system (Table S3-S4). Notably, bacteriophages from the class Caudoviricetes (tailed dsDNA

bacteriophages) accounted for the vast majority ( $>90$  %) of all samples (Fig. 1A, Table S3). The taxonomic classification rate of DNA viruses at the family level ranged from 22.1 % to 29.6 % across all samples (Table S4). Among the taxonomically classified viruses, Kyanoviridae (1.07 %  $\sim$  2.01 %), Peduoviridae (0.98 %  $\sim$  2.34 %), Inoviridae (0.82 %  $\sim$  2.31 %), Dolichocephalovirinae (0.88 %  $\sim$  2.04 %) and Adenoviridae (0.90 %  $\sim$  1.52 %) were generally the dominant families (Fig. S2A). Notably, more than 70 % of the DNA viruses could not be taxonomically classified at the family level.

From the metatranscriptomics analysis, 2,510 contigs that contained putative viral RdRp genes were identified, while 1,900 contigs were identified as incomplete RNA viral sequences lacking RdRp genes. Finally, a total of 1,864 unique putative RNA viral contigs were selected for further analysis. RNA viruses in this study were mainly divided into five phyla under the Riboviria domain: Lenarviricota (23.90 %  $\sim$  55.30 %), Duplornaviricota (16.54 %  $\sim$  42.61 %), Kitronoviricota (15.50 %  $\sim$  33.71 %), Pisuviricota (6.97 %  $\sim$  27.40 %), and Negarnaviricota (0.04 %  $\sim$  1.58 %). Additionally, p.0002.base-Kitrino, Artvervircota, and other unknown RNA viruses accounted for a small percentage ( $< 0.02$  %) of the total (Fig. 1A, Table S5). At the family level, the predominant RNA virus families included Narnaviridae (0.94 %  $\sim$  29.22 %), Totiviridae (14.92 %  $\sim$  42.24 %), Tombusviridae (2.61 %  $\sim$  7.80 %), Mitoviridae (7.06 %  $\sim$  24.53 %), and Potyviridae (0.16 %  $\sim$  9.78 %) (Fig. S2B, Table S6).

DNA viruses consistently exhibited a higher  $\alpha$ -diversity than RNA viruses, with the Shannon index values ranging from 8.24 to 9.18 for DNA viruses and from 2.41 to 4.07 for RNA viruses (Fig. 1B). Notable differences were observed in the  $\alpha$ -diversity trends with changes in DWT between DNA and RNA viruses. Overall, the  $\alpha$ -diversity of DNA viruses initially increased with the increase of DWT from  $-32 \sim -27$  cm to  $15 \sim 20$  cm, then slightly decreased with a further increase of DWT to  $45 \sim 50$  cm.

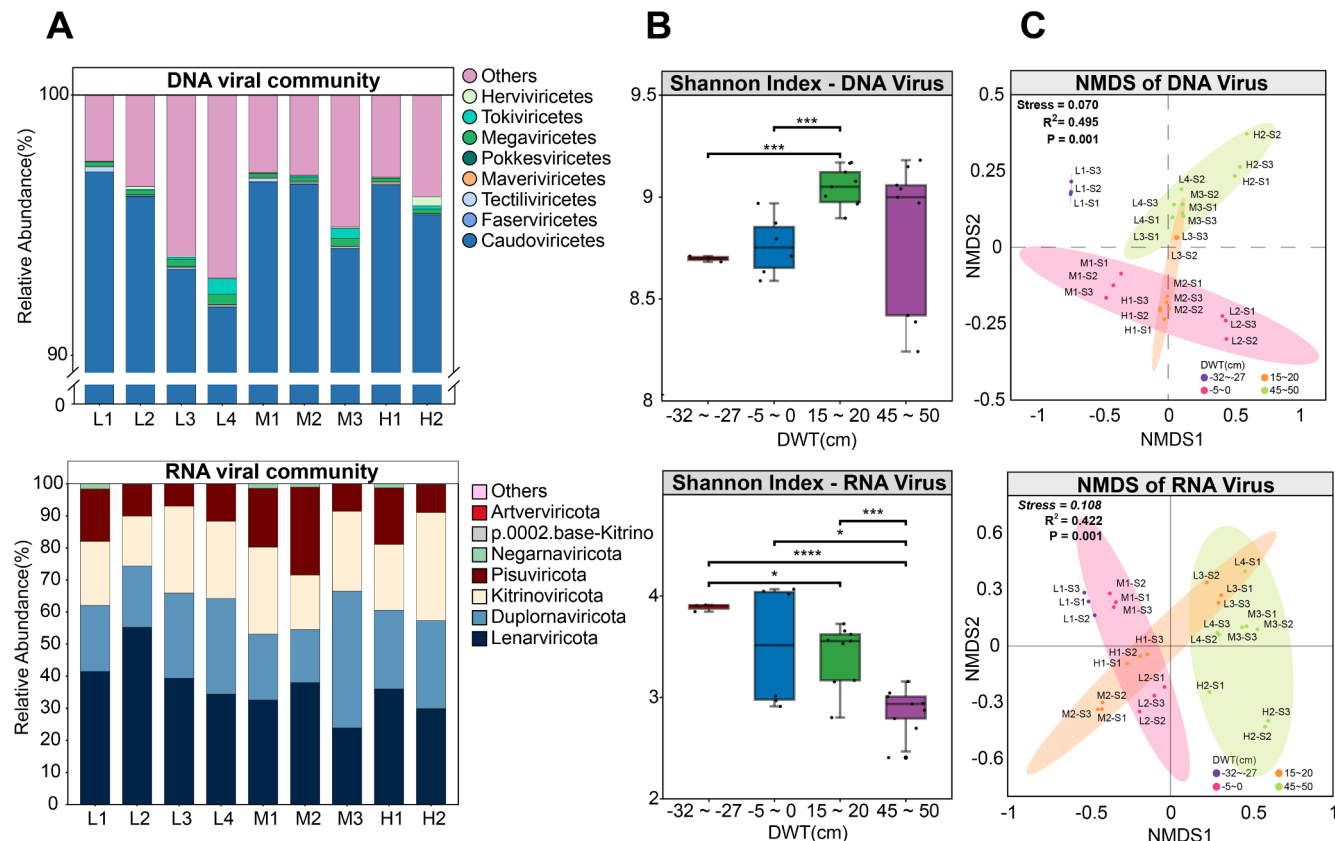


**Fig. 1.** Viral community composition and diversity at different DWT levels. (A) The composition of DNA and RNA viruses at class and phylum levels, respectively. (B-C)  $\alpha$ -diversity metrics represented by Shannon index, and  $\beta$ -diversity NMDS ordination of viral contigs across four DWTs based on Bray-Curtis dissimilarity. The asterisks indicate the level of statistical significance (\*  $p < 0.05$ , \*\*  $p < 0.01$ , \*\*\*  $p < 0.001$ , and \*\*\*\*  $p < 0.0001$ ).

50 cm, albeit non-significantly. In comparison to habitats above the water level ( $-32 \sim -27$  cm and  $-5 \sim 0$  cm), the  $\alpha$ -diversity index of the DNA viral community at a DWT of  $15 \sim 20$  cm is significantly ( $p < 0.001$ ) higher (Fig. 1B). Conversely, the  $\alpha$ -diversity of RNA viruses continuously decreased with increasing DWT (Fig. 1B). For the  $\beta$ -diversity at different DWTs of  $-32 \sim -27$  cm,  $-5 \sim 0$ ,  $15 \sim 20$  cm, and  $45 \sim 50$  cm, both DNA and RNA viruses exhibited distinct dispersion patterns and are clearly segregated from one another according to DWT levels (DNA virus:  $R^2 = 0.495$ ,  $p = 0.001$ ; RNA virus:  $R^2 = 0.422$ ,  $p = 0.001$ ; Fig. 1C).

### 3.2. AMG identification and functional annotation of viral genomes

In total, we identified a catalog of AMGs corresponding to 2,457 KEGG orthologs, spanning diverse metabolic pathways such as energy metabolism, and metabolism involving carbohydrate, amino acid, cofactors, vitamins (Fig. S3A). Notably, AMGs related to glycolysis, pyruvate metabolism, carbon fixation, short-chain fatty acids (propanoate and butanoate) metabolism, and  $\text{CH}_4$  metabolism were widespread (Fig. S3B). This underscores the ecological importance of viruses in peatland carbon metabolism. To further elucidate their role in biogeochemical cycles, we identified AMGs involved in methane ( $n = 52$ ), nitrogen ( $n = 9$ ), phosphorus ( $n = 2$ ), and sulfur ( $n = 16$ ) metabolism, with those related to methane oxidation and production found to be relatively abundant (Fig. 2).

Similar to community diversity, the functional diversity of DNA viruses also showed a relatively narrow range (6.49 to 7.10) but raised with the increase of DWT, peaking at DWT of  $15 \sim 20$  cm. Significant differences in functional diversity were observed at different DWTs ( $p < 0.05$ ; Fig. S4A and S4B). NMDS analysis based on Bray-Curtis dissimilarity of KEGG orthologs' relative abundance revealed clear segregation of viral functional components among different groups, with significant differences in functional components across DWT ( $R^2 = 0.437$ ,  $p = 0.001$ ; Fig. S4C). The relative abundance of methane metabolism AMGs

(MM AMGs) also showed clear segregation across different DWTs ( $R^2 = 0.434$ ,  $p = 0.001$ ; Fig. S4D). In contrast to DNA viruses, only 46 KEGG orthologs were identified from 1,864 unique RNA viruses, with several involved in energy metabolism (e.g., cytochrome c oxidase subunit III [*coxIII*], NADH-quinone oxidoreductase subunit G [*nuoG*]) and cysteine metabolism (e.g., cystathione beta-synthase [*CBS*]).

### 3.3. Association between environmental factors and composition of viral community and AMGs

Based on the Mantel test results, we observed significant correlations (Mantel's  $p \leq 0.001$ ) between both DNA and RNA viral communities and key environmental factors in the Dajiuju peatland, including Water- $\text{CH}_4$ , conductivity, Eh, pH,  $\cdot\text{OH}$ , TOC, and WC (Fig. 3A). The DWT exhibited the strongest correlation with both DNA (Mantel's  $r = 0.619$ ) and RNA (Mantel's  $r = 0.525$ ) viral communities, underscoring its crucial role in shaping the viral community composition. Additionally, the functional composition of AMGs, particularly the MM AMGs, was significantly correlated with WC, TOC, Water- $\text{CH}_4$ , and DWT, while the overall functional composition (Mantel's  $r = 0.543$ ) and MM AMGs (Mantel's  $r = 0.530$ ) were most strongly correlated with Water- $\text{CH}_4$ . Among environmental factors, DWT is positively correlated with pH, Water- $\text{CH}_4$  and TOC, and negatively correlated with Eh (Fig. 3A).

The impact of DWT on the  $\alpha$ -diversity of DNA viruses appeared to be significant but indirect, mediated through changes in Eh (with a coefficient of  $-0.99$ ). In contrast, DWT directly and significantly enhanced the  $\alpha$ -diversity of RNA viruses ( $-0.64$ ) and indirectly influenced their  $\alpha$ -diversity by modulating TOC content in peat ( $-0.89$ ). Additionally, DWT also directly affected community dissimilarity for both DNA ( $-0.35$ ) and RNA ( $0.98$ ) viruses. Changes in Eh and TOC levels were key indirect factors shaping viral community diversity and composition. However, DNA and RNA viruses exhibited distinct patterns in their effects on  $\text{CH}_4$  concentrations in pore water. In addition to directly changing the diversity of its own community ( $-0.80$ ), DNA viruses also

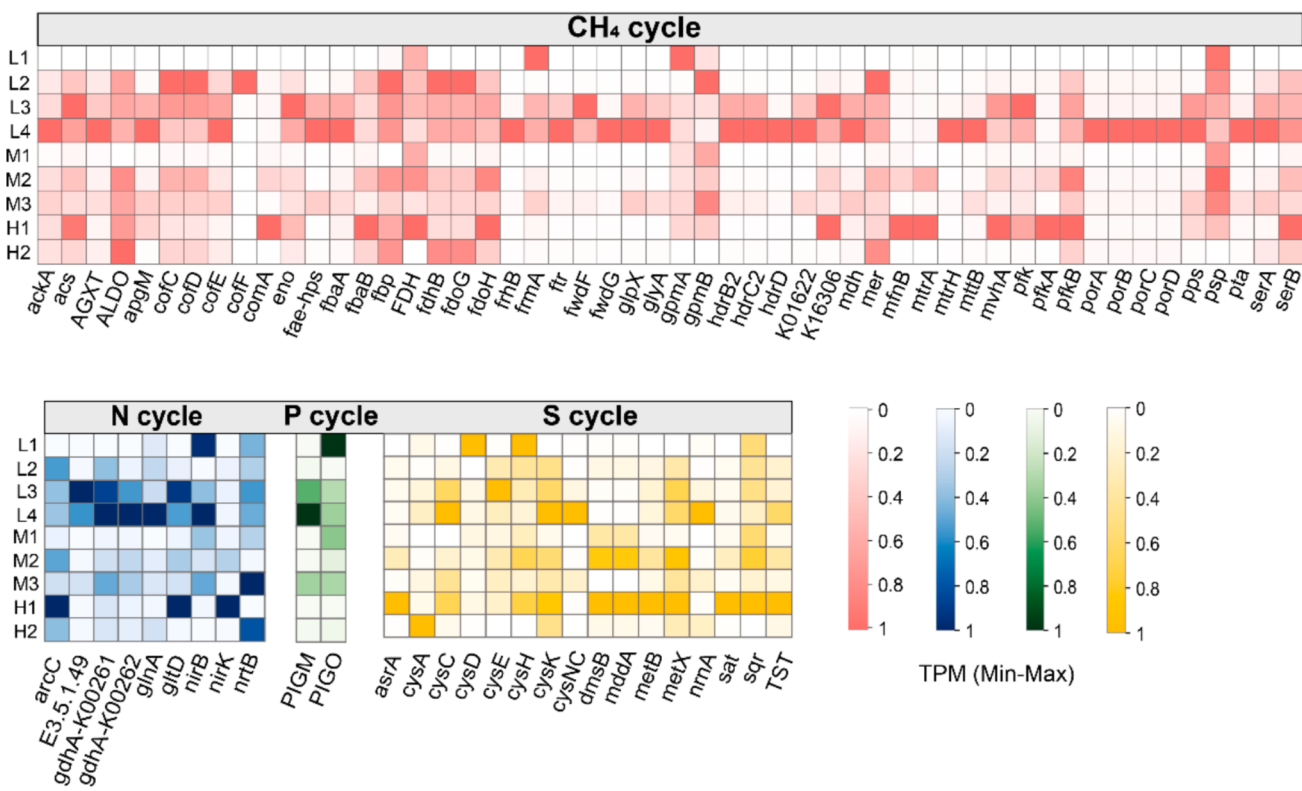


**Fig. 2.** Viral AMGs involved in methane (CH<sub>4</sub>), nitrogen (N), phosphorus (P) and sulfur (S) energy metabolism. Relative abundance of viral AMGs related to methane, nitrogen, phosphorus, and sulfur metabolism in various peatland sediment samples.

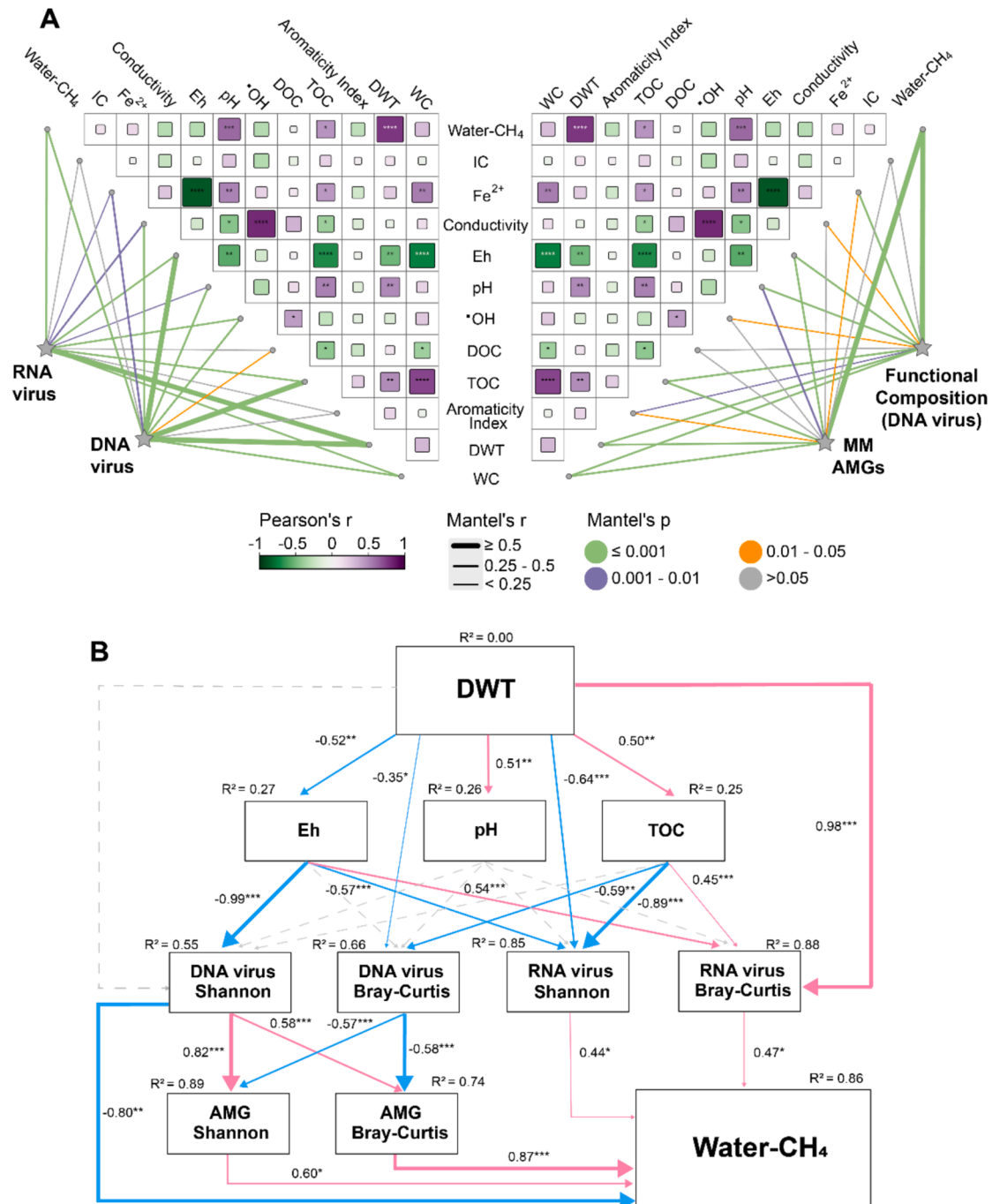


**Fig. 3.** Potential effects of environmental factors on viruses. (A) The correlation between environmental factors and DNA/RNA viral community composition is illustrated. The color gradient of Pearson's r values indicates the strength of the correlation between environmental factors. Both Mantel's r-value, indicated by the width of the edges, and Mantel's p-value, represented by the colors of the edges, reflect the strength and significance of the correlation, respectively. (B) Partial Least Squares Path Modeling (PLS-PM) analysis examines the influence pathways of DWT on viral community characteristics and Water-CH<sub>4</sub>. Red arrows indicate a significant positive effect, blue arrows represent a significant negative effect, and gray arrows denote no significant effects. The thickness of the arrows reflects the magnitude of the path coefficients in the model. MM AMGs: AMGs related to methane metabolism. \*  $p < 0.05$ , \*\*  $p < 0.01$ , \*\*\*  $p < 0.001$ .

tended to influence the Water-CH<sub>4</sub> by altering the diversity (0.60) and composition (0.87) of AMGs. In contrast, RNA viruses affected Water-CH<sub>4</sub> through variations in their own community diversity (0.44) and composition (0.47). Overall, DWT may influence viral community characteristics by altering the physicochemical properties of peat, thereby affecting Water-CH<sub>4</sub> (Fig. 3B).

### 3.4. Potential virus-host interaction

We identified 5,038 links between DNA viruses and prokaryotes. Only a small portion (~10 %) of the host taxa for the vOTUs has been predicted, covering 40 phyla and 309 families. These hosts predominantly belong to Acidobacteria ( $n = 288$ ), Pseudomonadota ( $n = 281$ ), and Bacteroidota ( $n = 183$ ) (Fig. 4A), which are also the predominant active microorganisms in the Dajiuju peatland (Fig. S5). Among all virus-host links, 630 vOTUs were predicted to infect single hosts, while

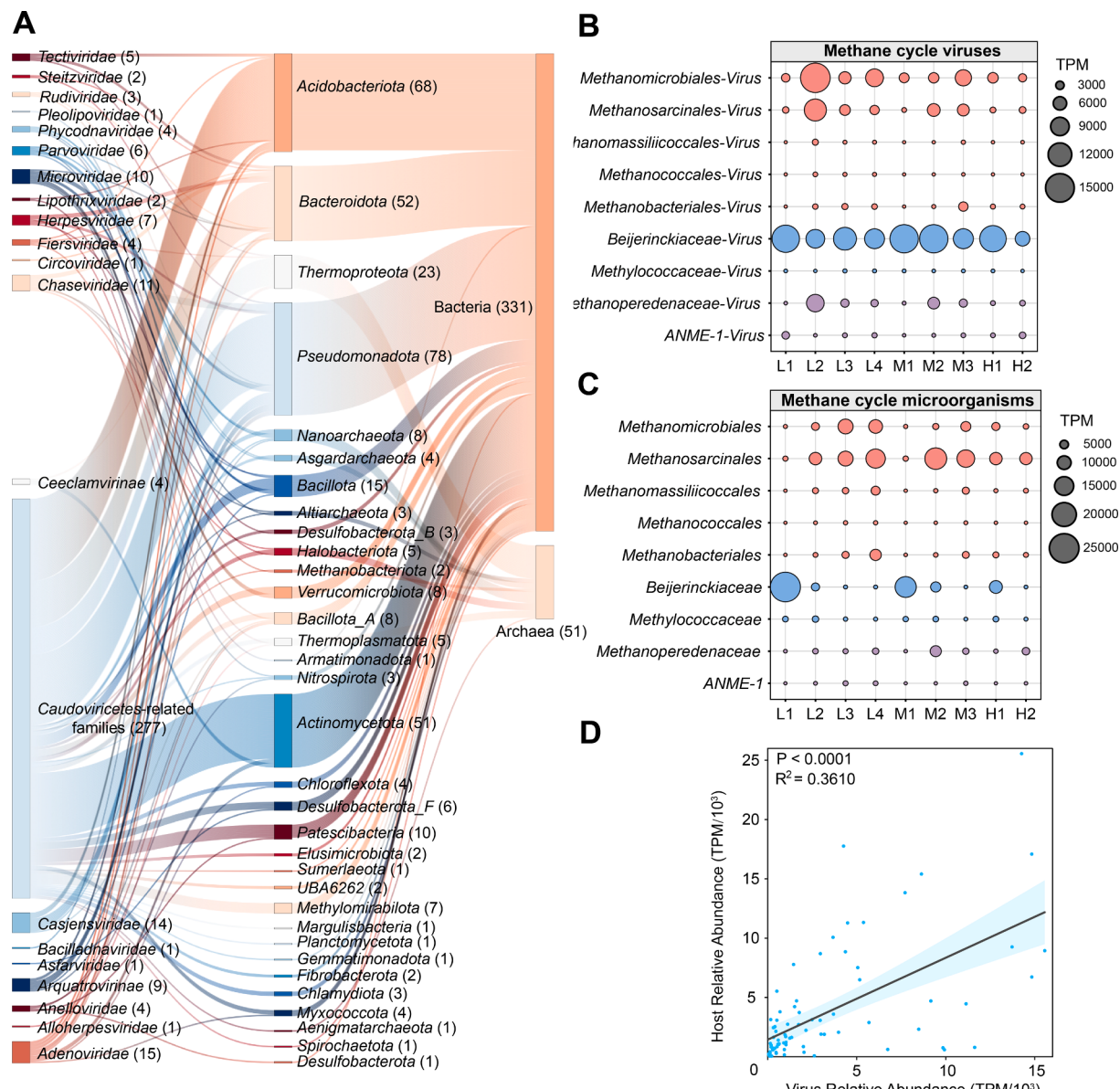


**Fig. 4.** Dynamic relationship between active hosts and viruses. (A) Predicted virus-host associations are shown at the levels of viral families (left), host phyla (middle) and host domains (right). Only linkages supported by PhaGCN2 annotation and iPhoP prediction are displayed. (B) Relative abundance of viruses represented by TPM value of microorganisms involved in CH<sub>4</sub> cycle. (C) Relative abundance of hosts represented by TPM value of microorganisms involved in CH<sub>4</sub> cycle. (D) Linear regression analysis between the abundance of microorganisms and corresponding viruses related to CH<sub>4</sub> cycle.

the remainder were associated with multiple distinct genera (Table S7). Notably, a small number of viruses were found to have the potential for cross-domain infection. Specifically, four viruses were predicted to infect both bacteria and archaea, with three of them capable of infecting *Bacteroidaceae* and some key archaea, such as *Nitrosphaerales* and *ANME-1* (Table S7).

Additionally, we identified active microbes involved in the CH<sub>4</sub> cycle and their corresponding viruses (Fig. 4B and 4C), including *Methanomicrobiales*, *Methanosarcinales*, *Methanomassiliicoccales*, *Methanococcales*, *Methanobacteriales*, *Beijerinckiaceae*, *Methylococcaceae*, *Methanoperedenaceae*, and *ANME-1*. *Methanomicrobiales* and *Methanosarcinales* were the predominant methanogenic archaea, while *Beijerinckiaceae* was the dominant methanotroph in peat environments, with their corresponding viruses also showing dominance (Fig. 4C). Linear regression analysis revealed a significant ( $p < 0.0001$ ) positive correlation between the relative abundance of microorganisms involved in the methane cycle and their corresponding viruses (Fig. 4D). Notably,

the abundance of *Beijerinckiaceae* and *Methanococcales* was significantly positively correlated with the abundance of their respective viruses (Fig. S6).

### 3.5. A wealth of potentially unknown viruses in peat environments

Conducted by a gene-sharing network, DNA viral sequences were assigned to viral clusters (VCs) corresponding to the genus level (Fig. 5A). In detail, 15,073 DNA vOTUs identified from the Dajihu peatland were compared to three data sets: i) 2,213 bacterial viruses and 91 archaeal viruses from RefSeq85, ii) 1,097 DNA vOTUs from peatland soils along a permafrost thaw gradient—Stordalen Mire peatland and iii) 4,569 vOTUs from SPRUCE peatland. All vOTUs collected from three peatlands and reference sequence (RefSeq85) were clustered into 4,213 VCs, while RefSeq85 alone formed 391 VCs. This suggests that peatland viruses remain largely unexplored. Although there are more shared VCs among different peat environments, only 7,923 vOTUs in Dajihu

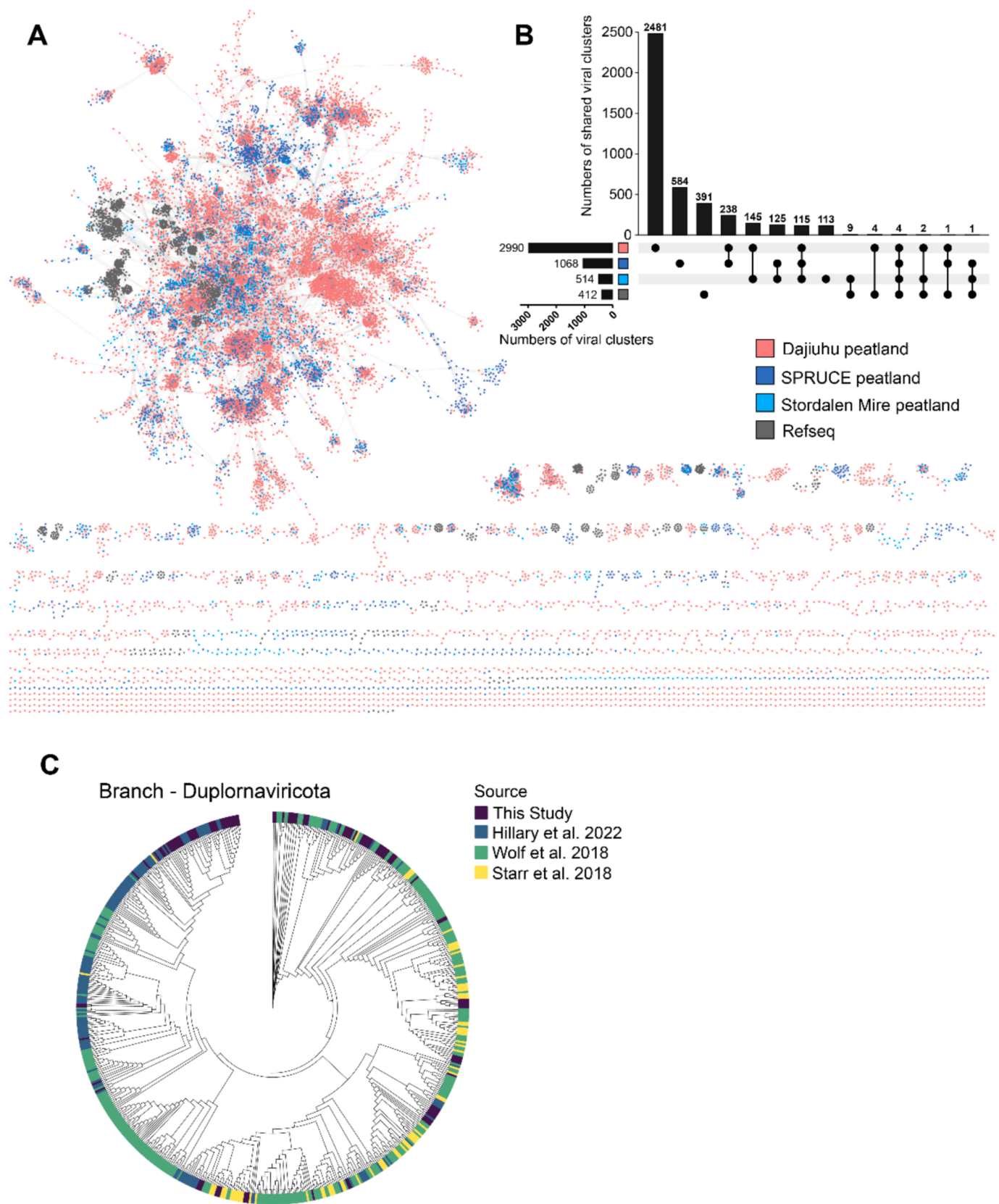


**Fig. 5.** Comparative analysis of viruses in Dajiuju peatland with viruses found in other habitats. (A) Gene-sharing network of DNA viral sequences collected from Dajiuju peatland, SPRUCE peatland, Stordalen Mire peatland and the RefSeq database. (B) The upset plot shows shared DNA viral clusters among different peatlands and the RefSeq database. (C) Phylogenetic analysis based on RNA viral RdRp genes (Phylum – Duplornaviricota).

peatland were clustered into 2,990 VCs (Fig. 5B, Table S8), while a subset of viruses lacks homologs in other peatlands and RefSeq85, indicating that DNA viruses in Dajiuju peatlands exhibit great specificity. For RNA virus, in comparison to reference RdRp sequences from Wolf et al. (Wolf et al., 2018), as well as RdRp sequence from bulk soil, leaves (Starr et al., 2019), peatland and different types of grassland (Hillary et al., 2022), many RNA viruses identified in this study at different phylum levels were found to be closely related viral blocks containing few reference sequences (Fig. 5C and Fig. S7). Phylogenetic analysis suggests the presence of unique RNA viruses in the Dajiuju peatland.

#### 4. Discussion

Compared to marine and terrestrial soil ecosystems, our understanding of viral communities and their functional roles in wetlands, particularly in peatlands, remains limited. While numerous studies have highlighted the impact of water table dynamics on peatland CH<sub>4</sub> emissions and distribution of methane-related microbiomes, few have investigated how viral communities respond to these dynamics. Given the high diversity and potential ecological functions of viruses observed in mangroves (Zhu et al., 2024), polar and mountain glaciers (Liu et al., 2023) and other important ecosystems (Luo et al., 2022), this study explores the diversity and activity of DNA and RNA viruses as well as their responses to hydrological variations in the Dajiuju peatland.

##### 4.1. Characteristics of viral communities and functions varied with changing DWT

In our study, *Caudoviricetes* was found to be the predominant viral class in the Dajiuju peatlands, aligning with its prevalence in other ecosystems such as soil and permafrost (Coclet et al., 2023; Ji et al., 2023). The widespread distribution of *Caudoviricetes* across different ecosystems reflected its extensive ecological adaptability and highlighted its significant role within these ecosystems. However, the limitations inherent in the classification system's completeness and annotation methods pose challenges in classifying peat viruses at the family or genus level, leaving many viruses still unassigned (ter Horst et al., 2021). Additionally, the DNA viruses in this study shared fewer VCs with viral sequences from public databases, while they shared relatively more VCs with viral sequences from other peatland environments (Fig. 5A and B). This discrepancy is likely attributable to the specific characteristics of peatland ecosystems.

Notably, as the DWT changes, distinct patterns of variation in the  $\alpha$ -diversity of DNA and RNA viruses were observed in the Dajiuju peatland (Fig. 1B), indicating the potential impact of the host preferences on viral community dynamics across different habitats. Specifically, RNA viruses primarily infect eukaryotes (Liang et al., 2023), including plants, animals, and fungi, which are more abundant in the surface layers of peatlands. Consequently, the  $\alpha$ -diversity of RNA viruses decreased with sample depth, consistent with that of eukaryotes (Fig. S8A). In contrast, DNA viruses have a broader host range, capable of infecting bacteria, archaea and eukaryotes (Carreira et al., 2024). As a result, no obvious correlation was observed between the  $\alpha$ -diversity of DNA viruses (Fig. 1B) and that of eukaryotes or prokaryotes individually (Fig. S8). In addition, the community diversity and functional diversity of DNA viruses raised with the increase of DWT, peaking at DWT of 15 ~ 20 cm. The Dajiuju Peatland experienced heavy rains during the week preceding our sampling, which raised its water table. Due to their proximity to the water table, the layers at a DWT of 15 ~ 20 cm were likely subjected to the most pronounced environmental changes during water table fluctuations. This dynamic condition creates a highly variable habitat, potentially fostering high microbial diversity in both community structure and functional potential. Consequently, it directly influences the community structure and functional diversity of the associated viruses, leading to the observed peak in functional diversity

at this depth.

Previous works have shown that environmental factors significantly influence the distribution patterns of viral communities, and these effects vary among habitats due to their specific characteristics (Luo et al., 2022; Ter Horst et al., 2023). For instance, nutrient content is a key driver of viral community composition in nutrient-limited soil environments (Huang et al., 2024). As a determining factor affecting CH<sub>4</sub> emissions from peatlands, water table dynamics significantly impact the composition and diversity of methane-related microbial communities in peatland ecosystems (Tian et al., 2024). This may result from fluctuations in groundwater levels altering hypoxic interfaces and redox conditions (Knief, 2019), leading to different distribution patterns of methane-related microbiomes (Wang et al., 2022b). In our study, the compositions of both DNA and RNA viral community were most strongly correlated with DWT (Fig. 3A). The influence of DWT on viral community diversity and composition may be indirectly mediated through changes in redox properties and TOC content (Fig. 3B). Furthermore, DNA and RNA viruses exhibit distinct effects on Water-CH<sub>4</sub> dynamics, with DNA viruses influencing these dynamics both directly and indirectly through the diversity of their own community and the community characteristics of their AMGs, whereas RNA viruses primarily affecting them through shifts in own community characteristics. This distinction may arise from the generally much fewer AMGs harbored on RNA viruses, a consequence of their smaller genome sizes and higher mutation rates compared to DNA viruses (Campillo-Balderas et al., 2015). Additionally, the inherent limitations of metatranscriptomic techniques hinder the recovery of complete RNA viral genomes from environmental samples, restricting our understanding of RNA viruses to shorter contigs. Consequently, investigating the functional roles of RNA viruses using metatranscriptomic remains a challenge. Notably, RNA viruses appeared to be more sensitive to changes in DWT. Despite limited knowledge about the ecological functions of RNA viruses, studies on marine ecosystems have found that RNA virus abundance is a strong predictor of marine carbon flux (Dominguez-Huerta et al., 2022). Given the significant impact of water table depth on CH<sub>4</sub> emissions, the high correlation between RNA virus communities and DWT suggests a potential ecological role for RNA viruses in carbon cycling within peatlands.

##### 4.2. Dynamics of host and virus abundance

In this study, the viral DNA was extracted from particulate particle viruses, which could actively infect and lysis hosts in the natural environment. Thus, metatranscriptomics may provide a more accurate depiction of active host-virus interactions than metagenomics, as metatranscriptomics analyzes actively expressed microbial communities by examining mRNA.

Hosts and viruses interact dynamically and complexly with varied infection modes. Typically, an increase in host abundance promotes viral replication and transmission, leading to a corresponding rise in virus abundance. However, excessive infection and lysis can reduce host abundance, which is inconducive to the proliferation of virus. In our study, the dynamics of virus and host abundance exhibited similar trends. Specifically, there is a positive correlation between the abundance of viruses associated with the CH<sub>4</sub> cycle and their corresponding hosts across various DWTs. Overall, a significant positive correlation was observed between the abundance of methane-cycling microorganisms and their corresponding viruses (Fig. 4D). Specifically, among methane-cycling microorganisms, *Beijerinckiaceae* and *Methanomicrobiales* were particularly abundant, with their corresponding viruses being also dominant (Fig. 4B and 4C). These findings highlighted the dynamic interplay between viral and host abundances, suggesting that viruses might alter their dominant taxa in response to host community characteristics, thereby potentially influencing methane cycling processes.

#### 4.3. Ecological potential of viruses on CH<sub>4</sub> cycling

Numerous studies have demonstrated the ability of viruses to acquire AMGs through horizontal gene transfer. Various glycoside hydrolase genes have been identified in viral genomes from peatland ecosystems, which are in charge of breaking down complex carbon compounds (Emerson et al., 2018; Trubl et al., 2018). It suggests that viruses in these environments may contribute to microbial carbon degradation, thus influencing CH<sub>4</sub> and CO<sub>2</sub> production. Although a substantial number of MM AMGs have been identified across 15 environments, including seven AMGs exclusively involved in methane metabolism, the majority of these MM AMGs is derived from mixed community metagenomes (Zhong et al., 2024), which may result in the loss of some viral signals during the sequencing process. Compared to previous studies, our findings reveal that viral genomes in Dajiuju peatland also harbor a diverse array of AMGs encoding enzymes involved in methanogenesis and CH<sub>4</sub> oxidation. While many AMGs may be involved in multiple metabolic pathways, we identified several that are exclusively associated with CH<sub>4</sub> cycling, such as *cofCDEF*, *mvhA*, *mtrA*, *fwdFG*, *mer* (Fig. 2), providing direct evidence of viral participation in CH<sub>4</sub> cycling. Moreover, the functional composition of DNA viruses, particularly those involved in CH<sub>4</sub> metabolism, exhibited a strong correlation with Water-CH<sub>4</sub>. Although the precise mechanisms by which viruses influence CH<sub>4</sub> cycling are not yet fully understood, this study underscores the significant ecological potential of viruses in driving biogeochemical cycles at the functional level.

Specifically, the *mvhA* gene involved in encoding the F<sub>420</sub>-non-reducing hydrogenase (MvhADG), which is commonly found in association with heterodisulfide reductases (HdrABC), forming a tight complex known as the HdrABC-MvhADG complex. This complex is capable of oxidizing hydrogen, and the produced H<sup>+</sup> can drive the reduction of ferredoxin in hydrogenotrophic methanogenesis pathway. This process is closely linked to the final step of methane generation, which involves the formation of CoM-S-S-CoB and CH<sub>4</sub>. Furthermore, the *mtrA* gene encodes a subunit of the Mtr enzyme complex, which transfers a methyl group to coenzyme M, forming methyl-CoM. This exergonic process drives sodium-ion translocation, supporting energy metabolism in methanogens that produce CH<sub>4</sub> from CO<sub>2</sub> or acetate (Harms et al., 1995). Additionally, the *cofC*, *cofD*, *cofE*, and *cofF* genes in methanogens are involved in the synthesis of the redox cofactor F<sub>420</sub>, which is primarily used in CH<sub>4</sub> production via CO<sub>2</sub>-reducing and methylotrophic pathways (Grinter and Greening, 2021). In detail, *cofC* and *cofD* are involved in the biosynthesis of F<sub>420</sub>, while *cofE* and *cofF* genes are responsible for producing mature F<sub>420</sub> by adding a γ-linked poly-glutamate tail and capping the γ-glutamyl tail, respectively (Grinter and Greening, 2021). Notably, our findings address the gap in Zhong et al.'s study by identifying the *cofC* and *cofD* genes in viral genomes (Zhong et al., 2024), highlighting the role of DNA viruses in methane production through the regulation of coenzyme F<sub>420</sub> synthesis. Furthermore, the discovery of the *mvhA* gene expends our understanding of the diversity of pathways through which viruses influence the methane cycle. Collectively, our studies suggest that viruses in the Dajiuju Peatland may influence key rate-limiting steps of the CH<sub>4</sub> cycle by encoding these AMGs.

Interestingly, AMGs related to the sulfur cycle were also prevalent across various samples (Fig. 2A), including genes encoding components of a transporter protein complex (*cysA*), adenylylsulfate kinase synthase (*cysC*), sulfate adenylyltransferase (*cysD*), phosphoadenosine phosphosulphate reductase (*cysH*), sulfate adenylyltransferase (*sat*), sulfide oxidoreductase (*sqr*), methanethiol S-methyltransferase (*mddA*), anaerobic sulphite reductase (*asrA*), and bifunctional oligoribonuclease and PAP phosphatase (*nrrA*). The *cysC*, *cysD*, *cysH* and *nrrA* genes are involved in assimilatory sulfate reduction, while the *sat* and *sqr* genes are associated with dissimilatory sulfur reduction and sulfur oxidation, respectively (Yu et al., 2021). Previous works have shown that some viruses can infect hosts crossing domains, including methanogens,

methanotrophic archaea (MMA) and *Deltaproteobacteria*. Species in the *Desulfuromonadales* order, which belong to the *Deltaproteobacteria* class, are mutualistic partners of MMA and are involved in the sulfur cycle (Wang et al., 2022a). Since sulfate is a key electron acceptor in anoxic environments and sulfur is crucial for biomass composition, viruses may influence host energy metabolism by providing AMGs involved in sulfur cycling, such as *cysH*, potentially helping hosts adapt to environmental stresses like the anoxic conditions in deep peat environments.

Despite the widespread presence of RNA viruses in nature, our understanding of their ecological functions remains less comprehensive than that of DNA viruses, to which extensive studies have been devoted. While many AMGs have been identified in DNA virus genomes, such genes are rare in RNA virus genomes (Dominguez-Huerta et al., 2022). Recently, a global survey of the RNA virome revealed that the AMGs carried by RNA viruses encompass multiple functional categories, including translation, energy metabolism, membrane transport, transcription, replication and repair, as well as signal transduction (Zhao et al., 2024). Notably, some identified AMGs are closely associated with biogeochemical cycles, such as central metabolism (e.g., *pk*, *acpP*, *speD*, and *metK*), sulfur metabolism (e.g., *soxY* and *soxZ*), nitrogen metabolism (e.g., *napA*, *nirB*, and *nirD*) and photosynthesis systems (e.g., *psbA*, *psbC*, *psbD*, and *psbJ*) (Dominguez-Huerta et al., 2022; Zhao et al., 2024). However, there is still insufficient evidence regarding the involvement of RNA viruses in other biogeochemical cycles, particularly the methane cycle, and their potential role in these cycles requires further investigation. In this study, we identified several genes involved in cellular energy metabolism (e.g., *coxlII*, *nuoG*) and cysteine metabolism (e.g., *CBS*) within RNA virus sequences (Fig. 6B). Notably, the *coxlII* gene encodes a core component of cytochrome c oxidase (Complex IV), which plays a crucial role in oxidative phosphorylation and ATP production, essential for maintaining cellular energy supply (Kadenbach, 2021). The *nuoG* gene encodes a subunit of NADH-quinone oxidoreductase, an enzyme crucial to mitochondrial oxidative phosphorylation, typically involved in intracellular electron transfer and ATP synthesis (Chadwick et al., 2018; Ohnishi et al., 2018). Interestingly, the *CBS* gene identified in this study has previously been shown to facilitate the degradation of methionine and redirect organic sulfur into the cysteine biosynthesis pathway (Miles and Kraus, 2004; Wang et al., 2022a). Cysteine is typically enriched in viral tail spike protein, which may be crucial for disrupting host membranes via both specific and non-specific electrostatic and hydrophobic interactions with cell surface groups (Shai, 2002; Thevissen et al., 2003). The *dcm* gene, also involved in the cysteine biosynthesis pathway, is widespread among MMA viruses (Wang et al., 2022a), suggesting that cysteine may play a crucial role in the viral impacts on the CH<sub>4</sub> cycle. However, further work is required to obtain more direct evidence regarding the involvement of RNA viruses in the methane cycle.

#### 5. Conclusions

This study reveals the critical role of DWT in regulating viral communities and activities in a subalpine peatland. It also highlights the potential ecological functions of both DNA and RNA viruses in the CH<sub>4</sub> cycle. Viral communities in the sediments of the Dajiuju peatland are highly sensitive to changes in DWT, redox potential, and TOC content, with DWT exhibiting the strongest correlation. Notably, DWT potentially modulates Water-CH<sub>4</sub> by altering the functional characteristics of DNA viruses and community traits of RNA viruses, respectively. Additionally, the abundant MM AMGs found in DNA viruses, especially those exclusively involved in the CH<sub>4</sub> cycle, provide compelling evidence for the involvement of DNA viruses in the CH<sub>4</sub> cycle. The composition of MM AMGs is significantly driven by the DWT. Furthermore, the discovery of functional genes related to energy metabolism and amino acid synthesis in RNA viruses sheds new light on their ecological significance. Given the intensification of global warming and the critical ecological role of peatlands in global carbon emissions, these findings provide new

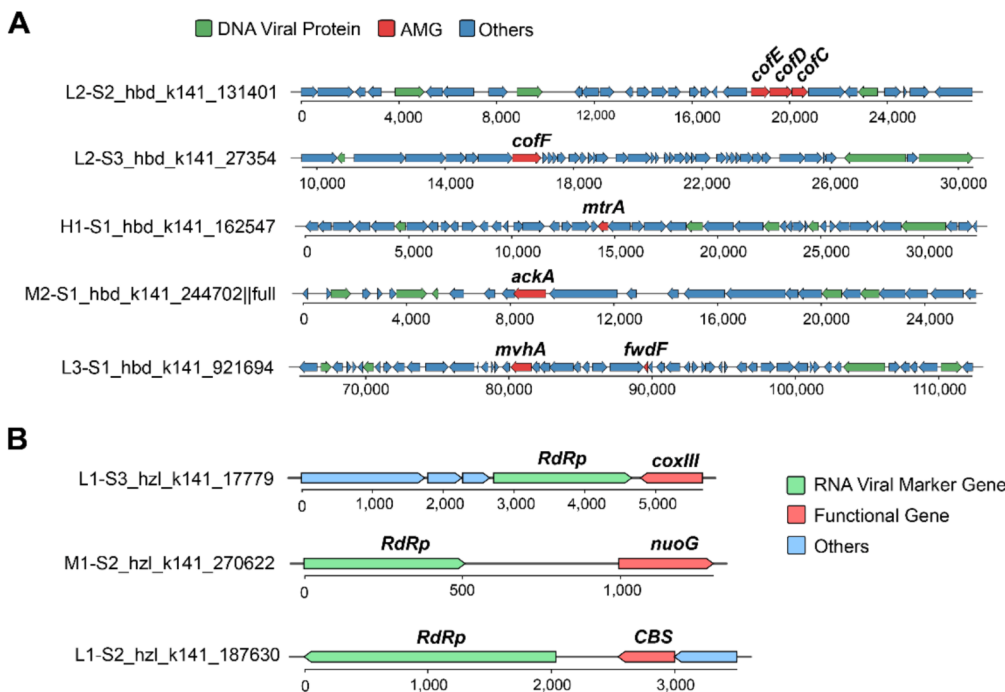


**Fig. 6.** (A) Genomic mapping of DNA viral sequences encoding AMGs associated with methane metabolism. (B) Genomic mapping of RNA viral sequences encoding functional genes related to energy metabolism and cysteine metabolism.

insights into how DWT affects viral communities in subalpine peatlands and offer important references for understanding the relationship between hydrological conditions and CH<sub>4</sub> emissions in these ecosystems.

#### CRediT authorship contribution statement

**Ziye Xiong:** Writing – original draft, Visualization, Validation, Software, Formal analysis. **Xuan Qiu:** Writing – review & editing, Supervision, Project administration, Methodology, Investigation, Funding acquisition, Conceptualization. **Xing Xiang:** Writing – review & editing, Validation. **Lanlan Cai:** Writing – review & editing, Validation. **Nian Wang:** Writing – review & editing, Validation. **Xiayu Huang:** Writing – review & editing, Validation. **Hongmei Wang:** Writing – review & editing, Validation.

#### Declaration of competing interest

The authors declare that they have no known competing financial interests or personal relationships that could have appeared to influence the work reported in this paper.

#### Acknowledgments

We would like to thank Liujun Cao, Guang Yang, Yuhang Wang and Mingming Zhang for the help in collecting the samples. We would also like to thank Liang Shen, Xiaoyu Cheng and Yanhong Wang for valuable discussion. Hefei Advanced Computing Center is thanked for providing computer resources. This work was supported by the National Natural Science Foundation of China (Grants U20A2094, 42425305, 42072336 and 42188102) and the Natural Science Foundation of Hubei Province, China (Grant 2024AFD383).

#### Appendix A. Supplementary data

Supplementary data to this article can be found online at <https://doi.org/10.1016/j.envint.2025.109363>.

#### Data availability

Data will be made available on request.

#### References

- Buchfink, B., Xie, C., Huson, D.H., 2015. Fast and sensitive protein alignment using DIAMOND. *Nat. Methods.* 12 (1), 59–60. <https://doi.org/10.1038/nmeth.3176>.
- Camargo, A.P., Roux, S., Schulz, F., Babinski, M., Xu, Y., 2023. Identification of mobile genetic elements with geNomad. *Nat. Biotechnol.* 42 (8), 1303–1312. <https://doi.org/10.1038/s41587-023-01953-y>.
- Campillo-Balderas, J.A., Lazcano, A., Becerra, A., 2015. Viral genome size distribution does not correlate with the antiquity of the host lineages. *Front. Ecol. Evol.* 3, 143. <https://doi.org/10.3389/fevo.2015.00143>.
- Cantalapiedra, C.P., Hernandez-Plaza, A., Letunic, I., Bork, P., Huerta-Cepas, J., 2021. eggNOG-mapper v2: functional annotation, orthology assignments, and domain prediction at the metagenomic scale. *Mol. Biol. Evol.* 38 (12), 5825–5829. <https://doi.org/10.1093/molbev/msab293>.
- Capella-Gutierrez, S., Silla-Martinez, J.M., Gabaldon, T., 2009. trimAl: a tool for automated alignment trimming in large-scale phylogenetic analyses. *Bioinformatics.* 25 (15), 1972–1973. <https://doi.org/10.1093/bioinformatics/btp348>.
- Carreira, C., Lonborg, C., Acharya, B., Aryal, L., Buiyidaite, Z., 2024. Integrating viruses into soil web biogeochemistry. *Nat. Microbiol.* 9 (8), 1918–1928. <https://doi.org/10.1038/s41564-024-01767-x>.
- Chadwick, G.L., Hemp, J., Fischer, W.W., Orphan, V.J., 2018. Convergent evolution of unusual complex I homologs with increased proton pumping capacity: energetic and ecological implications. *ISME J.* 12 (11), 2668–2680. <https://doi.org/10.1038/s41396-018-0210-1>.
- Chen, L.X., Meheust, R., Crits-Christoph, A., McMahon, K.D., Nelson, T.C., 2020. Large freshwater phages with the potential to augment aerobic methane oxidation. *Nat. Microbiol.* 5 (12), 1504–1515. <https://doi.org/10.1038/s41564-020-0779-9>.
- Chen, S., Zhou, Y., Chen, Y., Gu, J., 2018. fastp: an ultra-fast all-in-one FASTQ preprocessor. *Bioinformatics.* 34 (17), 884–890. <https://doi.org/10.1093/bioinformatics/bty560>.
- Coclet, C., Sorensen, P.O., Karaoz, U., Wang, S., Brodie, E.L., 2023. Virus diversity and activity is driven by snowmelt and host dynamics in a high-altitude watershed soil ecosystem. *Microbiome.* 11 (1). <https://doi.org/10.1186/s40168-023-01666-z>.
- Dominguez-Huerta, G., Zayed, A.A., Wainaina, J.M., Guo, J., Tian, F., 2022. Diversity and ecological footprint of global ocean RNA viruses. *Science.* 376 (6598), 1202–1208. <https://doi.org/10.1126/science.abn6358>.
- Emerson, J.B., Simon, R., Brum, J.R., Benjamin, B., Woodcroft, B.J., 2018. Host-linked soil viral ecology along a permafrost thaw gradient. *Nat. Microbiol.* 3 (8), 870–880. <https://doi.org/10.1038/s41564-018-0190-y>.
- Evans, C.D., Peacock, M., Baird, A.J., Arzt, R.R.E., Burden, A., 2021. Overriding water table control on managed peatland greenhouse gas emissions. *Nature.* 593 (7860), 548–552. <https://doi.org/10.1038/s41586-021-03523-1>.

- Finn, R. D., Clements, J., Eddy, S. R., 2011. HMMER web server: interactive sequence similarity searching. *Nucleic Acids Res.* 39 (Web Server issue), W29–W37. doi: 10.1093/nar/gkr367.
- Graziotin, A.L., Koonin, E.V., Kristensen, D.M., 2017. Prokaryotic Virus Orthologous Groups (pVOGs): a resource for comparative genomics and protein family annotation. *Nucleic Acids Res.* 45 (D1), 491–498. <https://doi.org/10.1093/nar/gkw975>.
- Gregory, A.C., Zayed, A.A., Conceicao-Neto, N., Temperton, B., Bolduc, B., 2019. Marine DNA viral macro- and microdiversity from pole to pole. *Cell.* 177 (5), 1109–1123. <https://doi.org/10.1016/j.cell.2019.03.040>.
- Grinter, R., Greening, C., 2021. Cofactor F<sub>420</sub> an expanded view of its distribution, biosynthesis and roles in bacteria and archaea. *FEMS Microbiol. Rev.* 45 (5), 1–46. <https://doi.org/10.1093/femsre/fuab021>.
- Guo, J., Bolduc, B., Zayed, A.A., Varsani, A., Dominguez-Huerta, G., 2021. VirSorter2: a multi-classifier, expert-guided approach to detect diverse DNA and RNA viruses. *Microbiome.* 9 (1), 37. <https://doi.org/10.1186/s41068-020-00990-y>.
- Harms, U., Weiss, D.S., Gartner, P., Linder, D., Thauer, R.K., 1995. The energy conserving N<sup>5</sup>-methyltetrahydromethanopterin:coenzyme M methyltransferase complex from Methanobacterium thermoautotrophicum is composed of eight different subunits. *Eur. J. Biochem.* 228 (3), 640–648. <https://doi.org/10.1111/j.1432-1033.1995.0640m.x>.
- Hillary, L.S., Adriaenssens, E.M., Jones, D.L., McDonald, J.E., 2022. RNA-viromics reveals diverse communities of soil RNA viruses with the potential to affect grassland ecosystems across multiple trophic levels. *ISME Commun.* 2 (1), 34. <https://doi.org/10.1038/s43705-022-00110-x>.
- Huang, X., Xue, J., Wang, X., Meyers, P.A., Huang, J., 2013. Paleoclimate influence on early diagenesis of plant triterpenes in the Dajiuju peatland, central China. *Geochim. Cosmochim. Acta.* 123, 106–119. <https://doi.org/10.1016/j.gca.2013.09.017>.
- Huang, X., Zhou, Z., Liu, H., Li, Y., Ge, T., 2024. Soil nutrient conditions alter viral lifestyle strategy and potential function in phosphorous and nitrogen metabolisms. *Soil Biol. Biochem.* 189, 109279. <https://doi.org/10.1016/j.soilbio.2023.109279>.
- Huang, Y., Ciais, P., Luo, Y., Zhu, D., Qu, L., 2021. Tradeoff of CO<sub>2</sub> and CH<sub>4</sub> emissions from global peatlands under water-table drawdown. *Nat. Clim. Change.* 11 (7), 618–622. <https://doi.org/10.1038/s41558-021-01059-w>.
- Hyatt, D., Chen, G.L., Locascio, P.F., Land, M.L., Larimer, F.W., 2010. Prodigal: prokaryotic gene recognition and translation initiation site identification. *BMC Bioinf.* 11 (1), 119. <https://doi.org/10.1186/1471-2105-11-119>.
- Jang, H.B., Bolduc, B., Zablocki, O., Kuhn, J.H., Roux, S., 2019. Taxonomic assignment of uncultivated prokaryotic virus genomes is enabled by gene-sharing networks. *Nat. Biotechnol.* 37 (6), 632–639. <https://doi.org/10.1038/s41587-019-0100-8>.
- Ji, M., Fan, X., Cornell, C.R., Zhang, Y., Yuan, M.M., 2023. Tundra soil viruses mediate responses of microbial communities to climate warming. *mBio.* 14 (2), e03009-e03022. <https://doi.org/10.1128/mbio.03009-22>.
- Jiang, J.-Z., Yuan, W.-G., Shang, J., Shi, Y.-H., Yang, L.-L., 2022. Virus classification for viral genomic fragments using PhaGCN2. *Briefings Bioinf.* 24 (1), bbac505. <https://doi.org/10.1093/bib/bbac505>.
- Kadenbach, B., 2021. Complex IV - The regulatory center of mitochondrial oxidative phosphorylation. *Mitochondrion.* 58, 296–302. <https://doi.org/10.1016/j.mito.2020.10.004>.
- Katoh, K., Misawa, K., Kuma, K., Miyata, T., 2002. MAFFT: a novel method for rapid multiple sequence alignment based on fast Fourier transform. *Nucleic Acids Res.* 30 (14), 3059–3066. <https://doi.org/10.1093/nar/gkf436>.
- Kneif, C., 2019. Diversity of methane cycling microorganisms in soils and their relation to oxygen. *Curr Issues Mol Biol.* 33, 23–56. <https://doi.org/10.21775/cimb.033.023>.
- Kopylova, E., Noé, L., Touzet, H., 2012. SortMeRNA: Fast and accurate filtering of ribosomal RNAs in metatranscriptomic data. *Bioinformatics.* 28 (24), 3211–3217. <https://doi.org/10.1093/bioinformatics/bts611>.
- Leifeld, J., Menichetti, L., 2018. The underappreciated potential of peatlands in global climate change mitigation strategies. *Nat. Commun.* 9 (1), 1071. <https://doi.org/10.1038/s41467-018-03046-6>.
- Li, D., Luo, R., Liu, C.-M., Leung, C.-M., Ting, H.-F., 2016a. MEGAHIT v1.0: A fast and scalable metagenome assembler driven by advanced methodologies and community practices. *Methods.* 102, 3–11. <https://doi.org/10.1016/j.ymeth.2016.02.020>.
- Li, H., Durbin, R., 2009. Fast and accurate short read alignment with Burrows-Wheeler transform. *Bioinformatics.* 25 (14), 1754–1760. <https://doi.org/10.1093/bioinformatics/btp324>.
- Li, Y., Ma, C., Zhou, B., Cui, A., Zhu, C., 2016b. Environmental processes derived from peatland geochemistry since the last deglaciation in Dajiuju, Shennongjia, central China. *Boreas.* 45 (3), 423–438. <https://doi.org/10.1111/bor.12168>.
- Liang, Y., Zheng, K., McMinn, A., Wang, M., 2023. Expanding diversity and ecological roles of RNA viruses. *Trends Microbiol.* 31 (3), 229–232. <https://doi.org/10.1016/j.tim.2022.12.004>.
- Liu, H., Gu, Y., Ge, J., Yu, Z., Xu, X., 2022. The response of the Dajiuju Peatland ecosystem to hydrological variations: Implications for carbon sequestration and peatlands conservation. *J. Hydrol.* 612, 128307. <https://doi.org/10.1016/j.jhydrol.2022.128307>.
- Liu, Y., Jiao, N., Xu Zhong, K., Zang, L., Zhang, R., 2023. Diversity and function of mountain and polar supraglacial DNA viruses. *Sci. Bull.* 68 (20), 2418–2433. <https://doi.org/10.1016/j.scib.2023.09.007>.
- Liu, Y., Zhang, Z., Jiao, N., Zhu, Y., Zhang, R., 2024. Diversity and ecological roles of RNA viral communities in the cryosphere of the Tibetan Plateau. *bioRxiv.* doi: 10.1101/2024.08.30.610425 (Preprint).
- Luo, X., Wang, P., Li, J., Ahmad, M., Duan, L., 2022. Viral community-wide auxiliary metabolic genes differ by lifestyles, habitats, and hosts. *Microbiome.* 10 (1), 190. <https://doi.org/10.1186/s40168-022-01384-y>.
- Lyu, Z., Shao, N., Akinyemi, T., Whitman, W.B., 2018. Methanogenesis. *Curr. Biol.* 28 (13), 727–732. <https://doi.org/10.1016/j.cub.2018.05.021>.
- Martin, M., 2011. Cutadapt removes adapter sequences from high-throughput sequencing reads. *Embdet J.* 17, 10–12. <https://doi.org/10.14806/ej.17.1.200>.
- Miles, E.W., Kraus, J.P., 2004. Cystathione  $\beta$ -synthase: structure, function, regulation, and location of homocystinuria-causing mutations. *J. Biol. Chem.* 279 (29), 29871–29874. <https://doi.org/10.1074/jbc.R400005200>.
- Minh, B.Q., Schmidt, H.A., Chernomor, O., Schrempf, D., Woodhams, M.D., 2020. IQ-TREE 2: new models and efficient methods for phylogenetic inference in the genomic era. *Mol. Biol. Evol.* 37 (5), 1530–1534. <https://doi.org/10.1093/molbev/msaa015>.
- Nayfach, S., Camargo, A.P., Schulz, F., Eloë-Fadrosch, E., Roux, S., 2020. CheckV assesses the quality and completeness of metagenome-assembled viral genomes. *Nat. Biotechnol.* 39 (5), 578–585. <https://doi.org/10.1038/s41587-020-00774-7>.
- Neri, U., Wolf, Y.I., Roux, S., Camargo, A.P., Lee, B., 2022. Expansion of the global RNA virome reveals diverse clades of bacteriophages. *Cell.* 185 (21), 4023–4037. <https://doi.org/10.1016/j.cell.2022.08.023>.
- Ohnishi, T., Ohnishi, S.T., Salerno, J.C., 2018. Five decades of research on mitochondrial NADH-quinone oxidoreductase (complex I). *Biol. Chem.* 399 (11), 1249–1264. <https://doi.org/10.1515/bch-2018-0164>.
- Pratama, A.A., Bolduc, B., Zayed, A.A., Zhong, Z.-P., Guo, J., 2021. Expanding standards in viromics: in silico evaluation of dsDNA viral genome identification, classification, and auxiliary metabolic gene curation. *PeerJ.* 9, e11447. <https://doi.org/10.7717/peerj.11447>.
- Ren, J., Song, K., Deng, C., Ahlgren, N.A., Fuhrman, J.A., 2020. Identifying viruses from metagenomic data using deep learning. *Quant. Biol.* 8 (1), 64–77. <https://doi.org/10.1007/s40484-019-01874>.
- Roux, S., Camargo, A.P., Coutinho, F.H., Dabdoub, S.M., Dutill, B.E., 2022. iPHoP: an Integrated Machine-Learning Framework to Maximize Host Prediction for Metagenome-Assembled Virus Genomes. *21* (4), e3002083. <https://doi.org/10.1371/journal.pbio.3002083>.
- Shai, Y., 2002. Mode of action of membrane active antimicrobial peptides. *Biopolymers.* 66 (4), 236–248. <https://doi.org/10.1002/bip.10260>.
- Starr, E.P., Nuccio, E.E., Pett-Ridge, J., Banfield, J.F., Firestone, M.K., 2019. Metatranscriptomic reconstruction reveals RNA viruses with the potential to shape carbon cycling in soil. *PNAS.* 116 (51), 25900–25908. <https://doi.org/10.1073/pnas.1908291116>.
- Steinegger, M., Söding, J., 2017. MMseqs2 enables sensitive protein sequence searching for the analysis of massive data sets. *Nat. Biotechnol.* 35 (11), 1026–1028. <https://doi.org/10.1038/nbt.3988>.
- Steward, G.F., Culley, A.I., Mueller, J.A., Wood-Charlson, E.M., Belcaid, M., 2013. Are we missing half of the viruses in the ocean? *ISME J.* 7 (3), 672–679. <https://doi.org/10.1038/ismej.2012.121>.
- ter Horst, A.M., Santos-Medellín, C., Sorensen, J.W., Zinke, L.A., Wilson, R.M., 2021. Minnesota peat viromes reveal terrestrial and aquatic niche partitioning for local and global viral populations. *Microbiome.* 9 (1). <https://doi.org/10.1186/s40168-021-01156-0>.
- ter Horst, A.M., Fudyma, J.D., Sones, J.L., Emerson, J.B., 2023. Dispersal, habitat filtering, and eco-evolutionary dynamics as drivers of local and global wetland viral biogeography. *ISME J.* 17 (11), 2079–2089. <https://doi.org/10.1038/s41396-023-01516-8>.
- Thauer, R.K., 2010. Functionalization of Methane in Anaerobic Microorganisms. *49* (38), 6712–6713. <https://doi.org/10.1002/anie.201002967>.
- Thevissen, K., Ferkett, K.K.A., Franois, I.E.J.A., Cammou, B.P.A., 2003. Interactions of antifungal plant defensins with fungal membrane components. *Peptides.* 24 (11), 1705–1712. <https://doi.org/10.1016/j.peptides.2003.09.014>.
- Tian, W., Wang, R., Wang, H., Xiang, X., Huang, X., 2024. Hydrology drives spatiotemporal patterns of methane microbial communities and methane emissions in a sub-alpine peatland, Central China. *Agric. for. Meteorol.* 353, 110050. <https://doi.org/10.1016/j.agrformet.2024.110050>.
- Tian, W., Wang, H., Xiang, X., Wang, R., Xu, Y., 2019. Structural variations of bacterial community driven by sphagnum microhabitat differentiation in a subalpine peatland. *Front. Microbiol.* 10, 1661. <https://doi.org/10.3389/fmicb.2019.01661>.
- Trubl, G., Jang, A.H.B., Roux, A.S., Emerson, J.B., Solonenko, N., 2018. Soil viruses are underexplored players in ecosystem carbon processing. *mSystems* 3 (5), e00076–e118. <https://doi.org/10.1128/mSystems.00076-18>.
- Trubl, G., Roux, S., Solonenko, N., Li, Y.-F., Bolduc, B., 2019. Towards optimized viral metagenomes for double-stranded and single-stranded DNA viruses from challenging soils. *PeerJ.* 7, e7265.
- Urayama, S.I., Takaki, Y., Nishi, S., Yoshida-Takashima, Y., Deguchi, S., 2018. Unveiling the RNA virosphere associated with marine microorganisms. *Mol. Ecol. Resour.* 18 (6), 1444–1455. <https://doi.org/10.1111/1755-0998.12936>.
- Wang, L., Wang, Y., Huang, X., Ma, R., Li, J., 2022a. Potential metabolic and genetic interaction among viruses, methanogen and methanotrophic archaea, and their syntrophic partners. *ISME Commun.* 2 (1), 50. <https://doi.org/10.1038/s43705-022-00135-2>.
- Wang, R., Wang, H., Xi, Z., Tuovinen, O.H., Gong, L., 2022b. Hydrology driven vertical distribution of prokaryotes and methane functional groups in a subtropical peatland. *J. Hydrol.* 608, 127592. <https://doi.org/10.1016/j.jhydrol.2022.127592>.
- Wolf, Y.I., Kazlauskas, D., Iranzo, J., Lucía-Sanz, A., Kuhn, J.H., 2018. Origins and evolution of the global RNA virome. *e02329-18 mBio.* 9 (6). <https://doi.org/10.1128/mBio.02329-18>.
- Woolhouse, M.E.J., Brierley, L., 2018. Epidemiological characteristics of human-infective RNA viruses. *Sci. Data.* 5, 180017. <https://doi.org/10.1038/sdata.2018.17>.
- Xie, J., Chen, Y., Cai, G., Cai, R., Hu, Z., 2023. Tree Visualization By One Table (tvBOT): a web application for visualizing, modifying and annotating phylogenetic trees. *Nucleic Acids Res.* 51 (W1), W587–W592. <https://doi.org/10.1093/nar/gkd359>.

- Yu, X., Zhou, J., Song, W., Xu, M., He, Q., 2021. SCycDB: A curated functional gene database for metagenomic profiling of sulphur cycling pathways. *Mol. Ecol. Resour.* 21 (3), 924–940. <https://doi.org/10.1111/1755-0998.13306>.
- Yu, Z., Beilman, D.W., Frolking, S., MacDonald, G.M., Roulet, N.T., 2011. Peatlands and their role in the global carbon cycle. *EOS Transactions*. 92 (12), 97–98. <https://doi.org/10.1029/2011eo120001>.
- Zayed, A.A., Wainaina, J.M., Dominguez-Huerta, G., Pelletier, E., Guo, J., 2022. Cryptic and abundant marine viruses at the evolutionary origins of Earth's RNA virome. *Science*. 376 (6589), 156–162. <https://doi.org/10.1126/science.abm5847>.
- Zhao, Y., Zhang, Z., Liu, P., Feng, M., Wen, R., 2024. Functional and evolutionary characterization of potential auxiliary metabolic genes (AMGs) of the global RNA virome. *bioRxiv*. Doi: 10.1101/2024.10.16.618626 (Preprint).
- Zhong, Z.P., Du, J., Kostlbacher, S., Pjevac, P., Orlic, S., 2024. Viral potential to modulate microbial methane metabolism varies by habitat. *Nat Commun.* 15 (1), 1857. <https://doi.org/10.1038/s41467-024-46109-x>.
- Zhu, Y., Li, R., Yan, S., Chen, X., Cen, S., 2024. Habitat- and lifestyle-dependent structural and functional characteristics of viruses in mangrove wetlands of different functional zonings. *Environ. Res.* 252, 119070. <https://doi.org/10.1016/j.envres.2024.119070>.
- Zhu, Y., Zhang, Y., Yan, S., Chen, X., Xie, S., 2023. Viral community structure and functional potential vary with lifestyle and altitude in soils of Mt. Everest. *Environ. Int.* 178, 108055. <https://doi.org/10.1016/j.envint.2023.108055>.